IDENTIFICATION OF DAMPING: PART 2, NON-VISCOUS DAMPING

S. ADHIKARI AND J. WOODHOUSE

Department of Engineering, University of Cambridge, Trumpington Street, Cambridge CB2 1PZ, England. E-mail: jw12@eng.cam.ac.uk

In a companion paper (see pp. 43–61 of this issue), it was shown that when a system is non-viscously damped, an identified equivalent viscous damping model does not accurately represent the damping behaviour. This demands new methodologies to identify non-viscous damping models. This paper takes a first step, by outlining a procedure for identifying a damping model involving an exponentially decaying relaxation function. The method uses experimentally identified complex modes and complex natural frequencies, together with the knowledge of the mass matrix for the system. The proposed method and several related issues are discussed by considering numerical examples of a linear array of damped spring-mass oscillators. It is shown that good estimates can be obtained for the exponential time constant and the spatial distribution of the damping.

© 2001 Academic Press

1. INTRODUCTION

Linear systems must generally be expected to exhibit non-viscous damping. In a companion paper [1] it was shown that when a system is non-viscously damped, it is possible to fit a viscous damping model to the set of measured transfer functions but that the fitted damping matrix will be non-symmetrical. The fitted model may also be misleading in other ways: for example, it may predict the wrong spatial distribution of damping over the structure. Of course, *a priori* selection of viscous damping in the identification procedure rules out any possibility of recognizing other damping behaviour present in the structure. In this paper, the identification of certain non-viscous damping models is considered in the context of general multiple degrees-of-freedom linear systems.

A key issue in identifying non-viscous damping is to decide on an appropriate damping model to consider. There have been detailed studies of material damping and of specific structural components. Lazan [2], Bert [3] and Ungar [4] have given excellent accounts of different mathematical methods for modelling damping in (solid) material and their engineering applications. The book by Nashif *et al.* [5] presents more recent studies in this area. There is a large body of literature on damping in composite materials where many researchers have evaluated a material's specific damping capacity. Baburaj and Matsuzaki [6] and the references therein give an account of research in this area. A more extensive list of references is given in Adhikari [7].

Other than material damping a major source of energy dissipation in a vibrating structure is the structural joints. Here, energy loss can take place through air-pumping and local frictional effects. The air-pumping phenomenon is associated with air trapped in pockets in the vicinity of a vibrating surface. In these situations, the air is squeezed in and

out through any available gap, leading to viscous dissipation of energy. Damping behaviour associated with joints has been studied by many authors. For example, Earls [8] has obtained the energy dissipation in a lap joint over a cycle under different clamping pressure. Beards and Williams [9] have noted that significant damping can be obtained by suitably choosing the fastening pressure to allow some interfacial slip in joints. In many cases, these damping mechanisms turn out to be locally non-linear, requiring an equivalent linearization technique for a global analysis [10]. These studies provide useful physical insights into damping mechanisms, but due to their very specific nature it is not possible to formulate a general procedure for the identification of such mechanisms by simple vibration measurement.

Banks and Inman [11] have proposed a somewhat general approach for identification of non-viscous damping models in Euler–Bernoulli beams. They have considered four different models of damping: viscous air damping, Kelvin–Voigt damping, time-hysteresis damping and spatial-hysteresis damping, and used a spline inverse procedure to form a least-squares fit to the experimental data. It was observed that the spatial hysteresis model combined with a viscous air damping model gave the best quantitative agreement with the experimental time histories. A procedure for obtaining hysteretic damping parameters in free-hanging pipe systems is given by Fang and Lyons [12]. Assuming material damping to be the only source of damping they have given a theoretical expression for the loss factor of the nth mode. Their theory predicts higher modal damping ratios in higher modes. The system-specific nature of these methods means that they cannot be extended in a simple way to more general multiple degrees-of-freedom systems.

Recently, Woodhouse [13] has discussed the general class of linear non-viscous damping models, in which damping forces are expressed in terms of the past history of the velocities via convolution integrals over suitable kernel functions. Such kernel functions are described under many different names in the literature of different subjects: for example, retardation functions, heredity functions, after-effect functions and relaxation functions. This model was originally introduced by Biot [14]. The viscous damping model is a special case of this general damping model when the kernel functions are delta functions, and thus have no memory. In reference [13], it was shown that for light damping, such damping models can be handled in a very similar way to viscous models, using a first order perturbation method. This motivates the development of procedures for the identification of more general linear damping models from standard vibration testing data.

A wide variety of mathematical expressions could be used for the kernel functions. Of these, the exponential function seems to be a particularly promising candidate. Cremer and Heckl [15] have written "Of the many after-effect functions that are possible in principle, only one — the so-called relaxation function—is physically meaningful". They go on to give a physical justification for this model, by which they mean the exponential case. The argument applies most convincingly to the case of material damping, rather than joint damping. An alternative mathematical rationalization can be given in terms of exponential contributions from the poles of frequency-response functions when the Fourier transform is inverted [16]. With this motivation, this paper concentrates on fitting exponential damping models to vibration data.

The analysis in this paper is restricted to linear system behaviour and it is assumed that the damping is light. In section 2, we briefly review the theory of determination of complex frequencies and modes based on the first order perturbation method when the system is non-viscously damped. Using these perturbation results, a method for identification of non-viscous damping models using complex modes and natural frequencies is proposed. It is assumed that the mass matrix of the structure is known—either directly from a finite element model or by means of modal updating based on experimental measurements.

Having the mass matrix attempts can be made to identify an exponential damping model consistent with the measured complex modes. In section 3, a procedure to obtain the *relaxation parameter* of an exponential damping model is outlined. Identification of the associated *damping coefficient matrix* is discussed in section 4. The proposed method is illustrated using simulated numerical examples directly comparable to those in the companion paper [1].

2. BACKGROUND OF COMPLEX MODES

In this section, general linear damping models are considered, described by convolution integrals of the generalized co-ordinates over appropriate kernel functions. Consider the equations of motion of free vibration

$$\mathbf{M}\ddot{\mathbf{y}}(t) + \int_{-\infty}^{t} \mathscr{G}(t - \tau)\dot{\mathbf{y}}(\tau)\,\mathrm{d}\tau + \mathbf{K}\mathbf{y}(t) = \mathbf{0}. \tag{1}$$

Here $\mathscr{G}(t)$ is an $N \times N$ matrix of kernel functions. It will be assumed that $\mathscr{G}(t)$ is a symmetric matrix so that reciprocity automatically holds. In the special case when $\mathscr{G}(t) = \mathbf{C}\delta(t)$, where $\delta(t)$ is the Dirac delta function, equation (1) reduces to the standard form for viscous damping. A restriction on the form of the kernel functions is imposed by the fact that the rate of energy dissipation given by

$$\mathscr{D}(t) = \frac{1}{2}\dot{\mathbf{y}}(t)^{\mathrm{T}} \int_{-\infty}^{t} \mathscr{G}(t - \tau)\dot{\mathbf{y}}(\tau)\,\mathrm{d}\tau, \tag{2}$$

where $(\cdot)^{\mathrm{T}}$ denotes matrix transpose, should be non-negative. Now, substituting $\mathbf{y}(t) = \mathbf{z}\exp[\mathrm{i}\lambda t]$ and rewriting equation (1) in the frequency domain, the eigenvalue equation can be expressed as

$$-\lambda_j^2 \mathbf{M}\mathbf{z}_j + \mathrm{i}\lambda_j \mathbf{G}(\lambda_j)\mathbf{z}_j + \mathbf{K}\mathbf{z}_j = \mathbf{0}, \tag{3}$$

where $\mathbf{G}(\lambda)$ is the Fourier transform of $\mathscr{G}(t)$. This is a non-linear eigenvalue problem. Note that, in contrast with the viscously damped case, the number of eigenvalues will not necessarily be equal to $2N$, since additional eigenvalues may be introduced by the form of the functions $\mathbf{G}(\lambda_j)$. Exact solutions of such eigenvalue problems are computationally very demanding and some kind of approximate method is required for further analysis. Woodhouse [13] has treated this problem using a first order perturbation method assuming the damping to be small. The main results are briefly described for further reference. Suppose the undamped problem has eigenvalues (natural frequencies) ω_j and eigenvectors (modes) $\mathbf{x}_j$. The complex eigenvalues can then be expressed as

$$\lambda_j \approx \pm \omega_j + \mathrm{i}G'_{jj}(\pm \omega_j)/2, \tag{4}$$

where $G'_{kl}(\omega_j) = \mathbf{x}_k^{\mathrm{T}}\mathbf{G}(\omega_j)\mathbf{x}_l$ is the frequency-dependent damping matrix expressed in normal co-ordinates. Since the inverse Fourier transform of $\mathbf{G}(\omega)$ must be real it must satisfy the condition $\mathbf{G}(-\omega) = \mathbf{G}(\omega)^*$, where $(\cdot)^*$ denotes complex conjugation. It follows that the eigenvalues of the generally damped system appear in pairs λ and $-\lambda^*$ (unless λ is purely imaginary). The first order approximate expression for the complex eigenvectors can be obtained in a way similar to that used for the viscously damped system (as was first given by

Rayleigh [17]). The result is

$$\mathbf{z}_j \approx \mathbf{x}_j + i \sum_{\substack{k=1 \\ k \neq j}}^{N} \frac{\omega_j G'_{kj}(\omega_j)}{(\omega_j^2 - \omega_k^2)} \mathbf{x}_k. \tag{5}$$

Note that the eigenvectors also appear in complex conjugate pairs. Since in general $G'_{kj}(\omega_j)$ will be complex, in contrast to the viscously damped case the real part of the natural frequencies and mode shapes do not coincide with the undamped ones. This fact will complicate the problem of fitting model parameters to experimental complex modes.

It is natural to consider first the idealized problem in which just one relaxation function is used for identification purposes. In that case, the general form of the kernel function in equation (1) reduces to

$$\mathscr{G}(t) = \mathbf{C}g(t), \tag{6}$$

where $g(t)$ is some damping function and $\mathbf{C}$ is a positive-definite coefficient matrix. The admissible form of $g(t)$ is restricted by the condition of non-negative energy loss given in equation (2). The damping model in equation (6) is physically realistic if the real part of the Fourier transform of the kernel function is non-negative within the driving frequency range, that is $\Re[G(\omega)] \geqslant 0$, $\forall \omega$. This can be easily shown. Rewriting equation (2) in the frequency domain and using (6), the rate of energy dissipation can be expressed as

$$D(\omega) = \frac{\omega^2}{2} \Re\{\mathbf{z}^{*\top} \mathbf{C} \mathbf{z} G(\omega)\}, \tag{7}$$

where $\Re(\cdot)$ represents the real part of $(\cdot)$ and $D(\omega)$ and $G(\omega)$ are the Fourier transform of $\mathscr{D}(t)$ and $g(t)$ respectively. A physically realistic model of damping must satisfy

$$D(\omega) \geqslant 0 \quad \text{or} \quad \frac{\omega^2}{2} \Re\{\mathbf{z}^{*\top} \mathbf{C} \mathbf{z} G(\omega)\} \geqslant 0 \tag{8}$$
$$\text{or} \quad \Re\{G(\omega)\} \geqslant 0$$

since for a real value of driving frequency $\omega^2 \geqslant 0$ and $\mathbf{z}$ can be chosen in a way that $\Re\{\mathbf{z}^{*\top} \mathbf{C} \mathbf{z}\} \geqslant 0$ as $\mathbf{C}$ is positive definite.

3. FITTING OF THE RELAXATION PARAMETER

As has been mentioned earlier, from the wide range of non-viscous damping models the exponential function seems a particularly good candidate. It satisfies condition (8) at all frequencies. In this section, a general method to fit the relaxation parameter of an exponential damping model using measured modal data is outlined.

3.1. THEORY

It is assumed that the damping has only one relaxation function, so that the matrix of kernel functions is of the form

$$\mathscr{G}(t) = \mu e^{-\mu t} \mathbf{C}, \tag{9}$$

where μ is the relaxation parameter and $\mathbf{C}$ is the associated coefficient matrix. The factor μ serves to normalize the kernel function (see section 3.2). Complex natural frequencies and

mode shapes for systems with this kind of damping can be obtained from equations (4) and (5). In view of the expression for damping given in equation (9) it is easy to see that the term $G'_{kj}(\omega_j)$ appearing in these equations can be expressed as

$$G'_{kj}(\omega_j) = \frac{\mu}{(\mu + i\omega_j)} C'_{kj} = \left[\frac{\mu^2}{(\mu^2 + \omega_j^2)} - i\frac{\mu\omega_j}{(\mu^2 + \omega_j^2)} \right] C'_{kj}, \tag{10}$$

where $C'_{kj} = \mathbf{x}_k^T \mathbf{C} \mathbf{x}_j$. Using this expression in equation (4), the jth complex natural frequency is given by

$$\lambda_j \approx \omega_j + i\frac{C'_{jj}}{2}\left[\frac{\mu^2}{(\mu^2 + \omega_j^2)} - i\frac{\mu\omega_j}{(\mu^2 + \omega_j^2)} \right]. \tag{11}$$

Similarly, from equation (5) the jth complex mode can be expressed as

$$\mathbf{z}_j \approx \mathbf{x}_j + \sum_{\substack{k=1 \\ k \neq 1}}^{N} \frac{\mu\omega_j}{(\mu^2 + \omega_j^2)} \frac{\omega_j C'_{kj}}{(\omega_j^2 - \omega_k^2)} \mathbf{x}_k + i\sum_{\substack{k=1 \\ k \neq 1}}^{N} \frac{\mu^2}{(\mu^2 + \omega_j^2)} \frac{\omega_j C'_{kj}}{(\omega_j^2 - \omega_k^2)} \mathbf{x}_k. \tag{12}$$

Suppose that $\hat{\lambda}_j$ and $\hat{\mathbf{z}}_j$ for $j = 1, 2, \ldots, m$ are the *measured* complex natural frequencies and modes. Write

$$\hat{\mathbf{z}}_j = \hat{\mathbf{u}}_j + i\hat{\mathbf{v}}_j. \tag{13}$$

Here $\hat{\mathbf{z}}_j \in \mathbb{C}^N$ where N denotes the number of measurement points on the structure and the number of modes considered in the study is m. In general, $m \neq N$, usually $N \geqslant m$. Assume that $\hat{\mathbf{x}}_j \in \mathbb{R}^N$ are the *undamped modes* and $\hat{\mu}$ is the relaxation parameter to be estimated from the experiment. In order to fit a damping model of the form of (9), equations (11) and (12) must be valid in conjunction with the experimental measurements $\hat{\lambda}_j$ and $\hat{\mathbf{z}}_j$. As an initial approximation it may be supposed that the real part of the complex natural frequencies are the same as the undamped natural frequencies:

$$\hat{\omega}_j^{(0)} = \mathfrak{R}(\hat{\lambda}_j). \tag{14}$$

For most practical cases it turns out that the above value of $\hat{\omega}_j^{(0)}$ is sufficiently accurate to carry out further analysis. However, an iterative method is presented later which may be used to update the value of $\hat{\omega}_j$ and remove the need for this approximation (see section 4.2 for details).

In view of equations (12) and (13) and considering that only m modes are measured, separating real and imaginary parts of $\hat{\mathbf{u}}_j$ gives

$$\hat{\mathbf{u}}_j = \mathfrak{R}(\hat{\mathbf{z}}_j) \approx \hat{\mathbf{x}}_j + \sum_{\substack{k=1 \\ k \neq j}}^{m} \tilde{A}_{kj}\hat{\mathbf{x}}_k \quad \text{where } \tilde{A}_{kj} = \frac{\hat{\mu}\hat{\omega}_j}{(\hat{\mu}^2 + \hat{\omega}_j^2)} B_{kj} \tag{15}$$

and

$$\hat{\mathbf{v}}_j = \mathfrak{I}(\hat{\mathbf{z}}_j) \approx \sum_{\substack{k=1 \\ k \neq j}}^{m} \tilde{B}_{kj}\hat{\mathbf{x}}_k \quad \text{where } \tilde{B}_{kj} = \frac{\hat{\mu}^2}{(\hat{\mu}^2 + \hat{\omega}_j^2)} B_{kj}. \tag{16}$$

Here the unknown constants B_{kj} are defined as

$$B_{kj} = \frac{\hat{\omega}_j C'_{kj}}{\hat{\omega}_j^2 - \hat{\omega}_k^2}. \tag{17}$$

It may be noted that in addition to B_{kj}, the relaxation constant $\hat{\mu}$ and the undamped modes $\hat{\mathbf{x}}_k$ are also unknown.

Combining equations (15) and (16) gives

$$\hat{\mathbf{u}}_j = \hat{\mathbf{x}}_j + \frac{\hat{\omega}_j}{\hat{\mu}}\hat{\mathbf{v}}_j. \tag{18}$$

From the preceding equation it is clear that if $\hat{\mu} \gg \hat{\omega}_j$, then $\hat{\mathbf{u}}_j \rightarrow \hat{\mathbf{x}}_j$. This implies that when the damping mechanism is near to viscous, the real part of each complex mode tends towards the corresponding undamped mode. Since the undamped modes are orthonormal with respect to the mass matrix, from equation (16) it may be observed that the imaginary part of each complex mode $\hat{\mathbf{v}}_j$ is $\mathbf{M}$-orthogonal to its corresponding undamped mode so that $\hat{\mathbf{v}}_j^{\mathrm{T}}\mathbf{M}\hat{\mathbf{x}}_j = 0$. Premultiplying equation (18) by $\hat{\mathbf{v}}_j^{\mathrm{T}}\mathbf{M}$ gives

$$\hat{\mathbf{v}}_j^{\mathrm{T}}\mathbf{M}\hat{\mathbf{u}}_j = \hat{\mathbf{v}}_j^{\mathrm{T}}\mathbf{M}\hat{\mathbf{x}}_j + \frac{\hat{\omega}_j}{\hat{\mu}}\hat{\mathbf{v}}_j^{\mathrm{T}}\mathbf{M}\hat{\mathbf{v}}_j. \tag{19}$$

Now, use of the orthogonality property of $\hat{\mathbf{v}}_j$ and $\hat{\mathbf{x}}_j$ leads to

$$\hat{\mu}_j = \frac{\hat{\omega}_j\hat{\mathbf{v}}_j^{\mathrm{T}}\mathbf{M}\hat{\mathbf{v}}_j}{\hat{\mathbf{v}}_j^{\mathrm{T}}\mathbf{M}\hat{\mathbf{u}}_j}. \tag{20}$$

The notation $\hat{\mu}_j$ has been used because for different choices of j on the right-hand side, in general, different values of $\hat{\mu}$ will be obtained. If in practice very similar values were obtained, this would confirm the initial assumption that the actual system has only one relaxation time. On the other hand, if significantly different values are obtained it would indicate that the assumed model needs to be extended. It is shown shortly that the pattern of variation of $\hat{\mu}_j$ can give some clues about the true underlying model. If it is wished to choose a single value of $\hat{\mu}$ to best represent a range of values found by this procedure, several alternatives could be considered:

1. Simply *select* a value of j, say $j = k \leqslant m$, to obtain $\hat{\mu}$. For this choice

$$\hat{\mu} = \frac{\hat{\omega}_k\hat{\mathbf{v}}_k^{\mathrm{T}}\mathbf{M}\hat{\mathbf{v}}_k}{\hat{\mathbf{v}}_k^{\mathrm{T}}\mathbf{M}\hat{\mathbf{u}}_k}. \tag{21a}$$

   How to select the value of k will be discussed in the next subsection.
2. Average the realizations of $\hat{\mu}$. For this choice

$$\hat{\mu} = \frac{1}{m_\mu}\sum_{j=1}^{m_\mu}\frac{\hat{\omega}_j\hat{\mathbf{v}}_j^{\mathrm{T}}\mathbf{M}\hat{\mathbf{v}}_j}{\hat{\mathbf{v}}_j^{\mathrm{T}}\mathbf{M}\hat{\mathbf{u}}_j}, \tag{21b}$$

   where $m_\mu \leqslant m$ is the number of terms to be retained.
3. Sum the numerator and denominator separately and take their ratio to obtain $\hat{\mu}$. For this choice

$$\hat{\mu} = \frac{\sum_{j=1}^{m_\mu}\hat{\omega}_j\hat{\mathbf{v}}_j^{\mathrm{T}}\mathbf{M}\hat{\mathbf{v}}_j}{\sum_{j=1}^{m_\mu}\hat{\mathbf{v}}_j^{\mathrm{T}}\mathbf{M}\hat{\mathbf{u}}_j}. \tag{21c}$$

This can best be illustrated via a numerical example.

3.2. SIMULATION METHOD

Numerical studies have been carried out using simulated systems identical to those used in the companion paper [1]. Figure (1) shows the model systems together with the numerical values used. For these parameter values, the resulting undamped natural
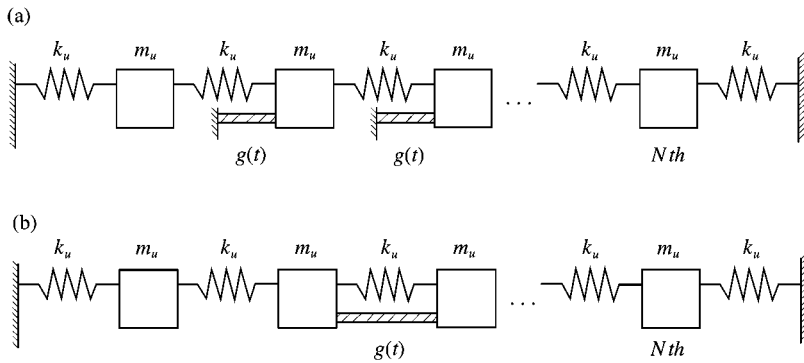
Figure 1. Linear array of N spring-mass oscillators, $N = 30$, $m_u = 1$ kg, $k_u = 4 \times 10^3$ N/m.

frequencies range from near zero to approximately 200 Hz. The damping elements are associated with masses between the sth and $(s + l)$th ($N = 30$, $s = 8$ and $(s + l) = 17$ are taken for the numerical calculations). For the system shown in Figure 1(a) the damping force depends only on the absolute motion of the individual masses. Such damping will be described as "locally reacting". For the system shown in Figure 1(b), by contrast, dissipative elements are connected between certain adjacent pairs of masses. In this case, the damping force depends on the relative motion of the two adjacent masses, and will be called "non-locally reacting". In the companion paper [1], a viscous damping matrix was calculated from the complex modes and frequencies of these systems. Here the parameters of an exponential damping model using the same modal data are to be identified.

The dissipative elements shown in Figure 1 are taken to be linear non-viscous dampers so that the equations of motion are described by (1). Three damping models, two of which were considered in Reference [1], are used: one with an exponential kernel function as assumed in the model being fitted, and two others with different functions to probe the limitations of the fitting procedure. They are determined by three different forms of $g(t)$ (defined in equation (6)):

- MODEL 1 (exponential):

$$g^{(1)}(t) = \mu_1 e^{-\mu_1 t}, \quad t \geqslant 0, \tag{22}$$

- MODEL 2 (Gaussian):

$$g^{(2)}(t) = 2\sqrt{\frac{\mu_2}{\pi}} e^{-\mu_2 t^2}, \quad t \geqslant 0, \tag{23}$$

- MODEL 3 (double exponential):

$$g^{(3)}(t) = \frac{\beta_1 \mu_3 e^{-\mu_3 t} + \beta_2 \mu_4 e^{-\mu_4 t}}{(\beta_1 + \beta_2)}, \quad t \geqslant 0. \tag{24}$$

All the three damping models are normalized such that the damping functions have unit area when integrated to infinity, i.e.,

$$\int_0^\infty g^{(j)}(t)\,dt = 1. \tag{25}$$

This will make them directly comparable with the viscous model, in which the corresponding damping function would be a unit delta function, $g(t) = \delta(t)$, and the coefficient matrix $\mathbf{C}$ would be the usual dissipation matrix. For each damping function a *characteristic time constant* can be defined via the first moment of $g^{(j)}(t)$:

$$\theta^{(j)} = \int_0^\infty t \, g^{(j)}(t) \, dt. \tag{26}$$

For the three damping models considered here, evaluating this integral gives

$$\theta^{(1)} = \frac{1}{\mu_1}, \quad \theta^{(2)} = \frac{1}{\sqrt{\pi \mu_2}}, \quad \theta^{(3)} = \frac{\beta_1/\mu_3 + \beta_2/\mu_4}{(\beta_1 + \beta_2)}. \tag{29}$$

Note that for viscous damping $\theta = 0$. The characteristic time constant of a damping function gives a convenient measure of "width": if it is close to zero the damping behaviour will be near viscous, and *vice versa*. For comparability between the three damping models all are taken to have the same time constant.

Complex natural frequencies and modes of the systems are calculated using equations (4) and (5), then these are treated as if they were experimental data obtained from a modal testing procedure. The procedures described above can be applied to identify the relaxation parameter of an exponential damping model. Results of the fitting procedure are presented for both small and large values of the characteristic time constant, expressed in non-dimensional form by

$$\theta = \gamma T_{min}, \tag{30}$$

where T_{min} is the period of the highest undamped natural frequency. When γ is small compared with unity the damping behaviour can be expected to be essentially viscous, but when γ is of order unity or bigger non-viscous effects are likely to be significant.

3.3. NUMERICAL RESULTS

3.3.1. *Results for small γ*

Consider first $\gamma = 0.02$, so that damping models show near-viscous behaviour. Since the viscous model is a special case of the exponential model good fit quality might be expected in this case. For the system shown in Figure 1(a) with locally reacting damping, Figure 2 shows the values of $\hat{\gamma}$ obtained from $\hat{\mu}$ (recall that $\hat{\gamma} = 1/T_{min}\hat{\mu}$) for all $j = 1, \ldots, 30$ for Gaussian damping (model 2). In the same figure, the values of $\hat{\gamma}$ corresponding to equations (21b) and (21c) using $m_\mu = 30$ are also shown. Because the damping mechanism is near to viscous the fitted values of $\hat{\gamma}$ are quite small, and in fact agree well with the assumed $\gamma = 0.02$ for all values of j. To obtain a single "best" value any one of the three relationships in equations (21a)–(21c) could be used. Similar features were observed (results not shown) when the fitting procedure was repeated for the non-locally damped case shown in Figure 1(b).

Now, attention turns to the systems with the double exponential damping model (model 3). It is supposed that the two exponential functions combine to give a value $\gamma = 0.02$. In this case, consider $\beta_1 = 0.5, \gamma_3 = 0.01$ and $\beta_2 = 0.5, \gamma_4 = 0.03$. Values of $\hat{\gamma}$ obtained for different modes for the locally reacting case with this damping model are shown in Figure 3. In the same figure, the values of $\hat{\gamma}$ corresponding to equation (21b) and (21c) are also shown. Again, as in the case of damping model 2 discussed above, the fitted values of $\hat{\gamma}$ are all very close to the correct value $\gamma = 0.02$. The only difference from the previous case is that values now
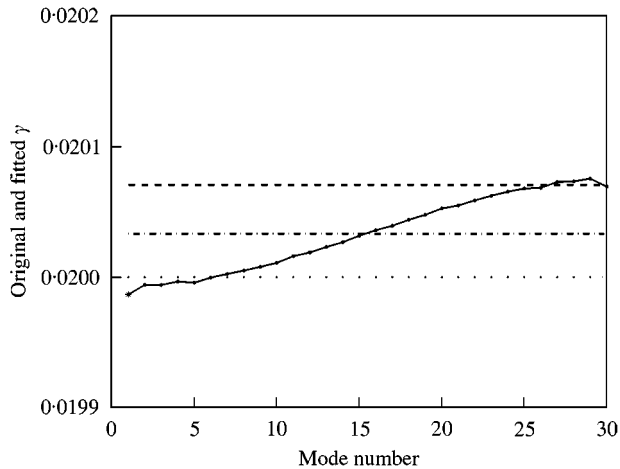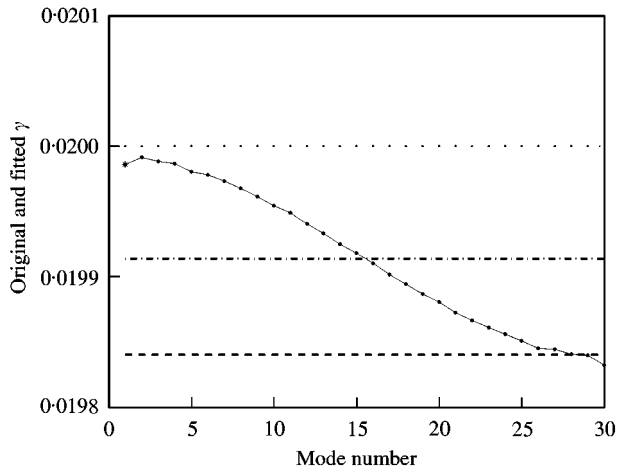
Figure 2. Values of $\hat{\gamma}$ obtained from different $\hat{\mu}$ calculated using equations (21a)–(21c) for the local case, damping model 2; (——), fitted $\hat{\gamma}$ for different modes; (·–··–·), fitted using equation (21b), $\hat{\gamma} = 0.020033$; (– –), fitted using equation (21c), $\hat{\gamma} = 0.020071$; (. . .), original $\gamma = 0.02$.

Figure 3. Values of $\hat{\gamma}$ obtained from different $\hat{\mu}$ calculated using equations (21a)–(21c) for the local case, damping model 3; (——), fitted $\hat{\gamma}$ for different modes; (·–··–·), fitted using equation (21b), $\hat{\gamma} = 0.019914$; (– –), fitted using equation (21c), $\hat{\gamma} = 0.019840$; (. . .), original $\gamma = 0.02$.

decrease slightly with j rather than increasing. Similar features were observed (results not shown) when the fitting procedure is extended to non-locally damped systems with damping model 3. It is concluded that, when the damping is near to viscous, regardless of the functional form or damping type, the fitting procedure gives a good estimate of the damping time constant and that any one of the relationships in equations (21a)–(21c) may be used to obtain the "best" relaxation parameter.

3.3.2. *Results for larger γ*

When γ is larger, the three damping models depart more strongly from the viscous damping model, each in its own way. Typical results for the case $\gamma = 0.5$ are shown. When
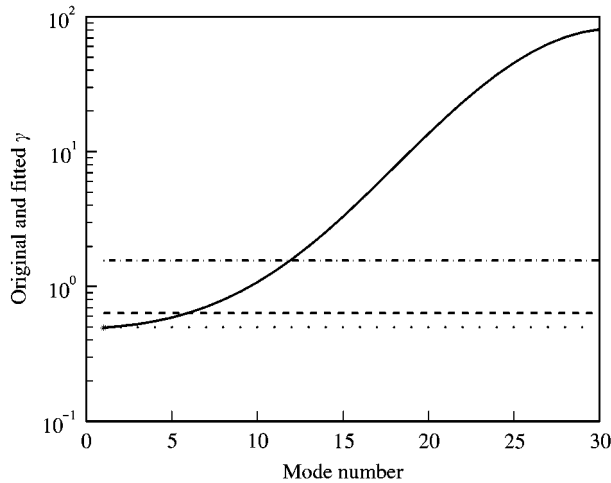
Figure 4. Values of $\hat{\gamma}$ obtained from different $\hat{\mu}$ calculated using equations (21a)–(21c) for the local case, damping model 2; (——), fitted $\hat{\gamma}$ for different modes; ($\cdot - \cdot$-), fitted using equation (21b), $\hat{\gamma} = 1{\cdot}5642$; (– –), fitted using equation (21c), $\hat{\gamma} = 0{\cdot}6367$; (. . .), original $\gamma = 0{\cdot}5$.

the fitting procedure is run for damping model 1, the calculation correctly reproduces the assumed γ value for all modes because the model being fitted is precisely the one assumed by the theory. This confirms the accuracy of the computer coding, but nothing further is to be learnt from displaying the results. Figure 4 shows the values of $\hat{\gamma}$ obtained for each mode for damping model 2 applied to the locally reacting system. The value of $\hat{\gamma}$ now varies considerably with j. This indicates, of course, that the assumption of a single kernel function is not correct for this system. As will be discussed shortly, the variation of $\hat{\gamma}$ with j gives some clue as to the correct form of the kernel function. Estimates of $\hat{\gamma}$ obtained from equations (21b) and (21c) using $m_\mu = 30$ are also shown in Figure 4. Both these estimates are higher than the value of γ used for simulation and also the estimate obtained using equation (21b) is higher than that obtained using equation (21c). Observe that the value of $\hat{\gamma}$ obtained using equation (21a) with $k = 1$ (marked by a $*$) is very close to the value of the original γ used in the simulation. An explanation of this behaviour is given in Appendix A. It is shown there that under rather general circumstances, a value of $\hat{\gamma}$ obtained from equation (21a) with $k = 1$ is likely to be a good estimate of the correct characteristic time constant defined via the first moment as in equation (30).

Results for the non-local case are shown in Figure 5. A similar trend is seen to that in Figure 4. In this figure it is also observed that the value of $\hat{\gamma}$ obtained from equation (21a) with $k = 1$ (marked by a $*$) is very close to the value of the original γ while those obtained from equations (21b) and (21c) differ significantly from the original one. Also, observe that estimates of $\hat{\gamma}$ obtained from the two former equations are higher than the simulated value for both the local and non-local systems. However, unlike the case of Figure (4), here the value of $\hat{\gamma}$ obtained from equation (21b) is lower than that obtained using equation (21c).

Now, consider damping model 3, consisting of two exponential functions. For the numerical values take: $\beta_1 = 0{\cdot}5$, $\gamma_3 = 0{\cdot}2$ and $\beta_2 = 0{\cdot}5$, $\gamma_4 = 0{\cdot}8$. This results in an equivalent γ for the model of $0{\cdot}5$, the same as for damping model 2 discussed above. Figure (6) shows the values of $\hat{\gamma}$ obtained for each mode for this damping model applied to the locally reacting system. This time $\hat{\gamma}$ decreases with j, in contrast to the Gaussian case. The range of variation is less dramatic, but still significant. Observe that, as with damping model 2, the value of $\hat{\gamma}$ obtained from equation (21a) with $k = 1$ (marked by a $*$) is very close to the
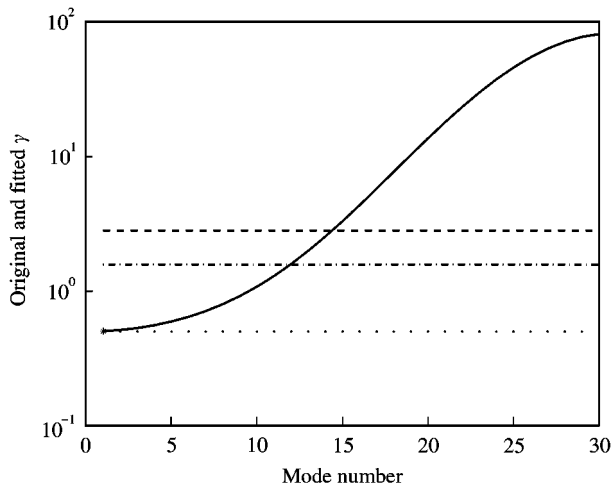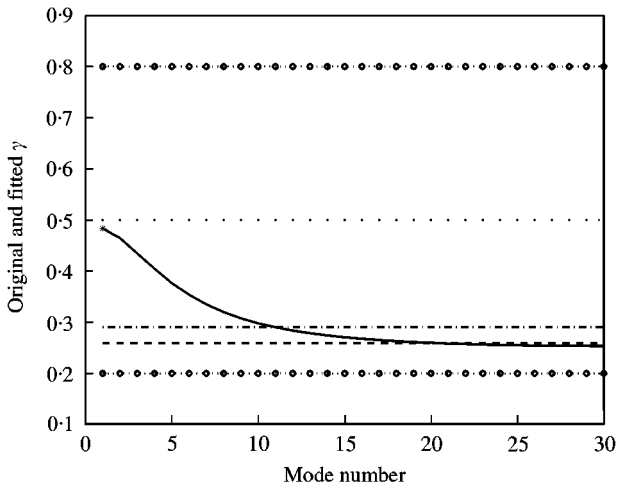
Figure 5. Values of $\hat{\gamma}$ obtained from different $\hat{\mu}$ calculated using equations (21a)–(21c) for the local case, damping model 2; (——), fitted $\hat{\gamma}$ for different modes; ($\cdot-\cdot$-), fitted using equation (21b), $\hat{\gamma} = 1\cdot5722$; (– –), fitted using equation (21c), $\hat{\gamma} = 2\cdot8130$; (. . .), original $\gamma = 0\cdot5$.

Figure 6. Values of $\hat{\gamma}$ obtained from different $\hat{\mu}$ calculated using equations (21a)–(21c) for the local case, damping model 3; (——), fitted $\hat{\gamma}$ for different modes; ($\cdot-\cdot$-), fitted using equation (21b), $\hat{\gamma} = 0\cdot2905$; (– –), fitted using equation (21c), $\hat{\gamma} = 0\cdot2590$; (. . .), original $\gamma = 0\cdot5$; ($\cdots\cdots$), γ for the two exponential functions.

value of the original γ used in the simulation while that obtained from equations (21b) and (21c) differ significantly from the original one. However, unlike the case of damping model 2, here the estimates of $\hat{\gamma}$ obtained from the two former equations are lower than the simulated value. Behaviour analogous to this was also observed when the identification procedure is repeated for the non-locally damped system.

3.4. DISCUSSION

It should be noted that for all the cases in Figures 2, 4, and 5, on the one hand, and Figures 3 and 6, on the other, the values of $\hat{\gamma}$ evaluated for each mode show the opposite

trend: for systems with damping model 2 the values of $\hat{\gamma}$ increase with increase of the mode number j, whereas for systems with damping model 3 the values of $\hat{\gamma}$ decrease with increase of the mode number. This behaviour can give further insight regarding the underlying damping function. Recall that after obtaining the complex modes and frequencies and having the mass matrix it is possible to obtain $\hat{\gamma}$ for different modes:

$$\hat{\gamma}_j = \frac{1}{T_{min}\,\hat{\mu}_j,} \tag{31}$$

where $\hat{\mu}_j$ is given by equation (20). Because by equation (30) it is known that $\hat{\gamma}_j$ is proportional to $\hat{\theta}_j$ it is sufficient only to understand the behaviour of the fitted $\hat{\theta}_j$. Using the expression of $\hat{\mu}_j$ in equation (A.13) of Appendix A, $\hat{\theta}_j$ can be expressed as

$$\hat{\theta}_j = \frac{1}{\hat{\mu}_j} = -\frac{F_I(\hat{\omega}_j)}{\hat{\omega}_j F_R(\hat{\omega}_j)}, \tag{32}$$

where F_R and F_I are, respectively, the real and imaginary parts of F, the Fourier transform of the (non-normalized) damping function $f(t)$ as defined in equation (A.1). Multiplying the numerator and denominator of equation (32) by the normalization constant β, the fitted $\hat{\theta}_j$ can be expressed in a more convenient form as

$$\hat{\theta}_j = \frac{G_I(\hat{\omega}_j)}{\hat{\omega}_j G_R(\hat{\omega}_j)}. \tag{33}$$

Here $G(\omega)$, the Fourier transform of the normalized damping function $g(t)$, is defined as

$$G(\omega) = \int_0^\infty g(t) e^{-i\omega t}\,dt. \tag{34}$$

Expanding $e^{-i\omega t}$ in the above expression gives

$$G(\omega) = \int_0^\infty g(t)\left[1 - i\,\omega t - \frac{\omega^2 t^2}{2!} + \frac{i\,\omega^3 t^3}{3!} - \cdots\right]dt$$
$$= \mathcal{M}_0 - i\,\omega\mathcal{M}_1 - \frac{\omega^2}{2}\mathcal{M}_2 + \frac{i\,\omega^3}{6}\mathcal{M}_3 - \cdots, \tag{35}$$

where $\mathcal{M}_k$, the kth moment of the damping function $g(t)$, is defined as

$$\mathcal{M}_k = \int_0^\infty t^k g(t)\,dt, \quad k = 0, 1, 2, \ldots. \tag{36}$$

For the three damping functions considered here in equations (22) and (23) the exact expressions for the kth moment may be obtained as follows:

- MODEL 1:

$$\mathcal{M}_k = k!\,\mu_1^{-k}, \quad k = 0, 1, 2, \ldots \tag{37}$$

- MODEL 2:

$$\mathcal{M}_{2k} = \frac{(2k-1)!!}{2\mu_2^k}, \quad \mathcal{M}_{2k+1} = \frac{k!}{\sqrt{\pi}}\,\mu_2^{-(k+1/2)}, \quad k = 0, 1, 2, \ldots \tag{38}$$

- MODEL 3:

$$\mathcal{M}_k = \frac{\beta_1\,k!\,\mu_3^{-k} + \beta_2\,k!\,\mu_4^{-k}}{(\beta_1 + \beta_2)}, \quad k = 0, 1, 2, \ldots \tag{39}$$
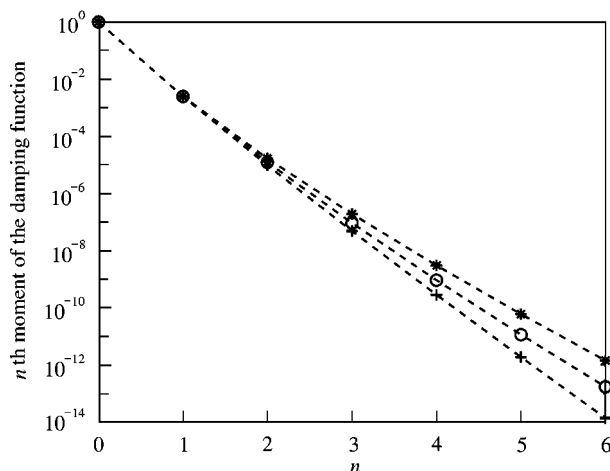
Figure 7. First six moments of the three damping functions for $\gamma = 0.5$; ($\cdot 0 \cdot$), model 1; ($\cdot + \cdot$), model 2; ($\cdot * \cdot$), model 3.

Clearly, for all the damping functions $\mathcal{M}_k > 0 \; \forall k$. In Figure 7, the first six moments of the three damping functions considered here are plotted when $\gamma = 0.5$. It is clear that although all $\mathcal{M}_k > 0$ their values approach zero as k increases. This ensures that omission of the higher order terms in equation (35) does not introduce much error for low values of ω. Now, separating real and imaginary parts of $G(\omega)$ in equation (35) gives

$$G_R(\omega) = \Re[G(\omega)] \approx \mathcal{M}_0 - \frac{\omega^2}{2} \mathcal{M}_2$$

$$G_I(\omega) = \Im[G(\omega)] \approx -\omega \mathcal{M}_1 + \frac{\omega^3}{6} \mathcal{M}_3. \tag{40}$$

Using these relationships, from equation (33) the value of $\hat{\theta}$ at any frequency can be obtained as

$$\hat{\theta}(\omega) \approx -\frac{-\omega \mathcal{M}_1 + (\omega^3/6)\mathcal{M}_3}{\omega(\mathcal{M}_0 - (\omega^2/2)\mathcal{M}_2)} = \frac{\mathcal{M}_1 - (\omega^3/6)\mathcal{M}_3}{\mathcal{M}_0 - (\omega^2/2)\mathcal{M}_2}$$

$$\approx \frac{1}{\mathcal{M}_0} \left\{ \mathcal{M}_1 - \frac{\omega^2}{6}\mathcal{M}_3 \right\} \left\{ 1 + \frac{\omega^2}{2}\left(\frac{\mathcal{M}_2}{\mathcal{M}_0}\right) + \frac{\omega^4}{4}\left(\frac{\mathcal{M}_2}{\mathcal{M}_0}\right)^2 + \cdots \right\}. \tag{41}$$

Since ω is small and $\mathcal{M}_0 > \mathcal{M}_2$, higher order terms arising in this expression will be small. Thus, neglecting all the terms associated with higher power than ω^2,

$$\hat{\theta}(\omega) \approx \frac{1}{\mathcal{M}_0} \left\{ \mathcal{M}_1 + \omega^2 \left(\frac{1}{2}\frac{\mathcal{M}_1 \mathcal{M}_2}{\mathcal{M}_0} - \frac{\mathcal{M}_3}{6} \right) \right\}. \tag{42}$$

The variation of the fitted θ_j in the low-frequency region can now be deduced. The curve of fitted θ_j will increase, as for the system with damping model 2 shown in Figures 2, 4 and 5, if

$$\frac{\mathcal{M}_1 \mathcal{M}_2}{\mathcal{M}_0} - \frac{\mathcal{M}_3}{3} > 0 \quad \text{or} \quad 3\frac{\mathcal{M}_2}{\mathcal{M}_3} - \frac{\mathcal{M}_0}{\mathcal{M}_1} > 0. \tag{43}$$

Conversely, the curve of fitted θ_j will decrease if the above quantity is negative. This analysis gives some insight into the nature of the underlying damping function. From Figure 7 or

equations (37)–(39) it may be seen that the damping functions considered here give behaviour which agrees with this condition.

4. FITTING OF THE COEFFICIENT MATRIX

4.1. THEORY

Once the relaxation parameter of the damping function is estimated the next step is to obtain the coefficient matrix $\mathbf{C}$ as shown in equation (9). After obtaining $\hat{\mu}$, from the imaginary part of equation (11) the diagonal entries of $\mathbf{C}'$ can be obtained as

$$C'_{jj} = 2\Im(\hat{\lambda}_j) \frac{(\hat{\mu}^2 + \hat{\omega}_j^2)}{\hat{\mu}^2}. \tag{44}$$

This C'_{jj} and $\hat{\mu}$ can be substituted into equation (11) and subsequently an improved estimate value of $\hat{\omega}_j$ may be obtained from (14) by

$$\hat{\omega}_j^{(new)} = \hat{\omega}_j + \frac{C'_{jj}}{2} \frac{\hat{\mu}\hat{\omega}_j}{(\hat{\mu}^2 + \hat{\omega}_j^2)} \tag{45}$$

If all the $\hat{\omega}_j^{(new)}$ are sufficiently close to $\hat{\omega}_j^{(0)}$ then the values of $\hat{\omega}_j^{(new)}$ can be taken as the estimated values, i.e., $\hat{\omega}_j = \hat{\omega}_j^{(new)}$. Otherwise the process can be repeated by substituting $\hat{\omega}_j^{(new)}$ in place of $\hat{\omega}_j$ in one of equations (21a)–(21c) to obtain $\hat{\mu}$, and subsequently obtaining a new set of $\hat{\omega}_j$ from (45). This iterative procedure may be continued until the differences between all new $\hat{\omega}_j$ and old $\hat{\omega}_j$ become sufficiently small. The final values of $\hat{\omega}_j$ and $\hat{\mu}$ are selected as the estimated values.

Now, $\hat{\mu}$ can be substituted in equation (18) to obtain an estimate of the undamped modes as

$$\hat{\mathbf{x}}_j = \hat{\mathbf{u}}_j - \frac{\hat{\omega}_j}{\hat{\mu}} \hat{\mathbf{v}}_j. \tag{46}$$

After obtaining $\hat{\mathbf{x}}_j$, in this way from equation (16), the constants $\tilde{B}_{kj}$ can be derived using Galerkin error minimization as described in section 3 of the companion paper [1]. Denoting $\tilde{\mathbf{B}} \in \mathbb{R}^{m \times m}$ as the matrix of unknown $\tilde{B}_{kj}$ gives

$$\tilde{\mathbf{B}} = [\hat{\mathbf{X}}^T\hat{\mathbf{X}}]^{-1}\hat{\mathbf{X}}^T\hat{\mathbf{V}}, \tag{47}$$

where

$$\hat{\mathbf{X}} = [\hat{\mathbf{x}}_1, \hat{\mathbf{x}}_2, \dots, \hat{\mathbf{x}}_m] \in \mathbb{R}^{N \times m} \tag{48}$$

is the matrix of undamped modes. Now, the off-diagonal terms C'_{kj} can be obtained from

$$C'_{kj} = \frac{(\hat{\omega}_j^2 - \hat{\omega}_k^2)}{\hat{\omega}_j} \frac{(\hat{\mu}^2 + \hat{\omega}_j^2)}{\hat{\mu}^2} \tilde{B}_{kj}, \quad k, j = 1, \dots, m, \quad k \neq j. \tag{49}$$

The diagonal entries of $\mathbf{C}'$ have already been obtained in equation (44). Recall that C'_{kj} are constant coefficients of the damping matrix in the modal co-ordinates, with associated time function $e^{-\hat{\mu}t}$. The coefficients in the original co-ordinates can be calculated using the transformation

$$\mathbf{C} = [(\hat{\mathbf{X}}^T\hat{\mathbf{X}})^{-1}\hat{\mathbf{X}}^T]^T\mathbf{C}'[(\mathbf{X}^T\hat{\mathbf{X}})^{-1}\hat{\mathbf{X}}^T] \in \mathbb{R}^{m \times m}. \tag{50}$$

This coefficient matrix together with the relaxation parameter completely defines the fitted damping model for the structure. This fitting procedure has made use only of the complex

natural frequencies, mode shapes and mass matrix to identify the best exponential damping model associated with the measurements.

It is easy to check that when $\hat{\mu}$ is large, i.e., when the damping mechanism is near to viscous, this procedure reduces exactly to the procedure described in the earlier paper [1] for identification of a viscous damping model. Thus, this method is a generalization of identification of viscous damping properties to the more general linear damping case described by an exponential model with a single relaxation time constant. One limitation of this method compared to the identification method for the viscous damping matrix is that an estimate of the mass matrix is required. The extra information from the mass matrix also enables one to detect whether the correct damping model of the system is viscous/ exponential or not.

4.2. SUMMARY OF THE IDENTIFICATION METHOD

In summary, the procedure can be described by the following steps:
1. Measure a set of transfer functions $H_{ij}(\omega)$ at a set of N grid points. Fix the number of modes to be retained in the study, say m. Determine the complex natural frequencies $\hat{\lambda}_j$ and complex mode shapes $\hat{z}_j$ from the transfer functions, for all $j = 1, \ldots, m$. Denote by $\hat{Z} = [\hat{z}_1, \hat{z}_2, \ldots, \hat{z}_m] \in \mathbb{C}^{N \times m}$ the complex mode-shape matrix. Set $\hat{U} = \Re[\hat{Z}] = [\hat{u}_1, \hat{u}_2, \ldots, \hat{u}_m]$ and $\hat{V} = \Im[\hat{Z}] = [\mathbf{v}_1, \hat{v}_2, \ldots, \hat{v}_m]$.
2. Obtain the first guess (i.e., $r = 0$) of the 'undamped natural frequencies' as $\hat{\omega}_j^{(r)} = \Re(\hat{\lambda}_j)$.
3. Estimate the relaxation parameter $\hat{\mu}^{(r)} = \hat{\omega}_1^{(r)} \hat{v}_1^T \mathbf{M} \hat{v}_1 / \hat{v}_1^T \mathbf{M} \hat{u}_1$ (or use a different estimate of $\hat{\mu}$ given by equation (21b) or (21c)).
4. Calculate the diagonal terms of the $\mathbf{C}'$ matrix as $C_{jj}^{\prime(r)} = 2\Im(\hat{\lambda}_j)(\hat{\mu}^{(r)^2} + \hat{\omega}_j^{(r)^2})/\hat{\mu}^{(r)^2}$ for all j.
5. Obtain new values of the undamped natural frequencies

$$\hat{\omega}_j^{(r+1)} = \hat{\omega}_j^{(r)} + \frac{C_{jj}^{\prime(r)}}{2} \frac{\hat{\mu}^{(r)} \hat{\omega}_j^{(r)}}{(\hat{\mu}^{(r)^2} + \hat{\omega}_j^{(r)^2})}.$$

6. Select a value of ε, say $\varepsilon = 0{\cdot}001$. If $|\hat{\omega}_j^{(r+1)} - \hat{\omega}_j^{(r)}| < \varepsilon \ \forall j$ then $\hat{\omega}_j = \hat{\omega}_j^{(r+1)}$, $C'_{jj} = C_{jj}^{\prime(r)}$ and $\hat{\mu} = \hat{\mu}^{(r)}$ and move to the next step. Otherwise, increase r, set the final values of $\hat{\omega}_j$ as the current values, i.e., $\hat{\omega}_j^{(r)} = \hat{\omega}_j^{(r+1)}$, and go back to step 3.
7. For all $j = 1, \ldots, m$ calculate the 'undamped mode shapes' $\hat{x}_j = \{\hat{u}_j - (\omega_j/\hat{\mu})\hat{v}_j\}$. Set $\hat{X} = [\hat{x}_1, \hat{x}_2, \ldots, \hat{x}_m] \in \mathbb{R}^{N \times m}$.
8. Evaluate the matrix $\tilde{B} = [\hat{X}^T \hat{X}]^{-1} \hat{X}^T \hat{V}$.
9. From the $\tilde{B}$ matrix get

$$C'_{kj} = \frac{(\hat{\omega}_j^2 - \hat{\omega}_k^2)(\hat{\mu}^2 + \hat{\omega}_j^2)}{\hat{\omega}_j} \frac{}{\hat{\mu}^2} \tilde{B}_{kj} \quad \text{for } k, j = 1, 2, \ldots, m, \quad k \neq j.$$

10. Use

$$\mathbf{C} = [(\hat{X}^T X)^{-1} \hat{X}^T]^T \mathbf{C}'[(\hat{X}^T \hat{X})^{-1} \hat{X}^T]$$

to get the coefficient matrix in physical co-ordinates.

It may be observed that even if the measured transfer functions are reciprocal, from this procedure there is no reason why the fitted coefficient matrix $\mathbf{C}$ will always be symmetric. If indeed a non-symmetric $\mathbf{C}$ is detected then it may be guessed that the physical law behind the damping mechanism in the structure cannot be described by an exponential model. This possibility will be illustrated by considering numerical examples.

4.3. NUMERICAL RESULTS

4.3.1. *Results for small γ*

Consider first $\gamma = 0.02$ so that all the damping models show near-viscous behaviour. For the system shown in Figure 1(a), with locally reacting damping, Figure (8) shows the fitted coefficient matrix of the exponential model for damping model 2, calculated using the complete set of 30 modes. The fitted matrix identifies the damping in the system very well. Equation (21a) with $k = 1$ has been used to obtain the relaxation parameter. As was seen in Figure 2, the fitted relaxation parameter $\hat{\gamma} = 0.02$ so that the fitted characteristic time constant also agrees exactly with the original one, even though the underlying model was Gaussian rather than exponential. The high portion of the plot corresponds exactly to the spatial location of the dampers. The off-diagonal terms of the identified damping matrix are very small compared to the diagonal terms, indicating correctly that the damping is locally reacting.

Now, consider the system shown in Figure 1(b) with non-locally reacting damping. Figure 9 shows the fitted coefficient matrix of an exponential model for damping model 2, using the full set of modes. Again the high portion of the plot corresponds to the spatial location of the dampers. Now, the negative off-diagonal terms in the identified damping matrix indicate that the damping is non-locally reacting. It is concluded that in both cases the proposed method extracts accurate information from the complex frequencies and modes. In practice, one might expect to be able to use only the first few modes of the system to identify the damping matrix. The proposed method can be applied using a smaller number of modes, and it is found that the result behaves in a very similar way to the case of identification of a viscous damping matrix as discussed in the companion paper [1]—the spatial resolution of the identified coefficient matrix gradually deteriorates as the number of modes used to fit the damping matrix is reduced, but still the identified coefficient matrix shows a reasonable approximation to the true behaviour.

When the fitting procedure is repeated using other damping models with a similarly short characteristic time constant, the results are very similar. The detailed difference in their functional behaviour does not influence the results significantly. It may be observed that the results obtained here are quite similar to those obtained by fitting a viscous damping model
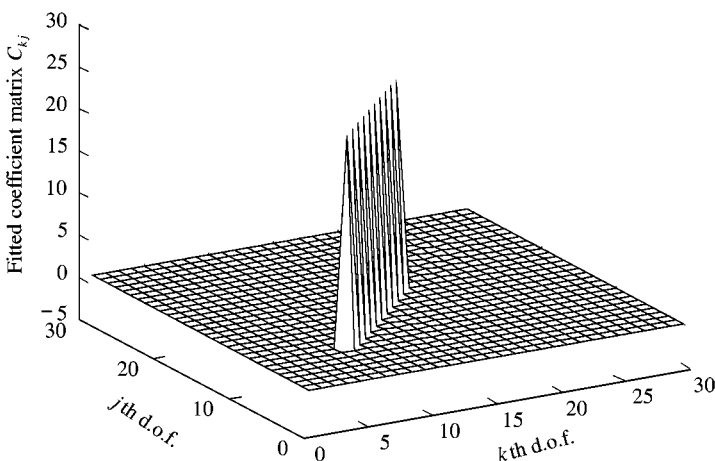

Figure 8. Fitted coefficient matrix of the exponential model for the local case, $\gamma = 0.02$, damping model 2.
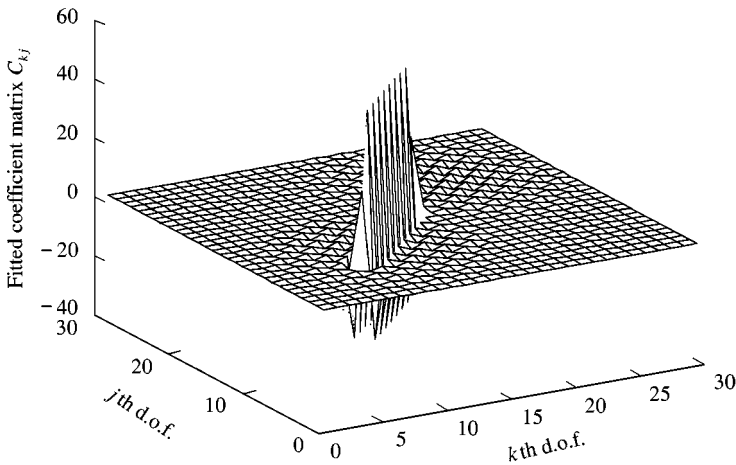
Figure 9. Fitted coefficient matrix of the exponential model for the non-local case, $\gamma = 0.02$, damping model 2.
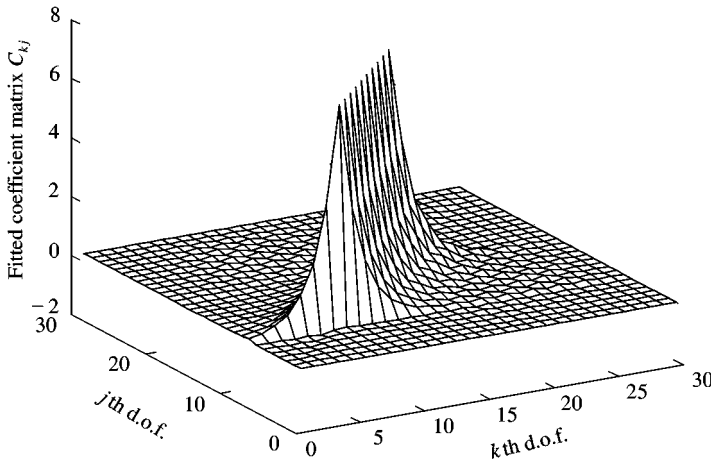

Figure 10. Fitted viscous damping matrix for the local case, $\gamma = 0.5$, damping model 1.

for the corresponding case discussed in section 4.1 of the companion paper [1]. In summary, it can be said that when the time constant for a damping model is small the proposed identification method seems to work well regardless of the functional form of the damping mechanism. The spatial location of damping is revealed clearly and the associated relaxation parameter is accurately estimated whether damping is locally or non-locally reacting. Modal truncation blurs the fitted coefficient matrix, but does not degrade the estimate of the relaxation parameter and overall the identification process remains valid.

4.3.2. *Results for larger* γ

When γ is larger the two non-exponential damping models depart from the exponential damping model, each in its own way. For the value $\gamma = 0.5$, Figure 10 shows the result of fitting a viscous damping matrix, using the procedure described in the companion paper
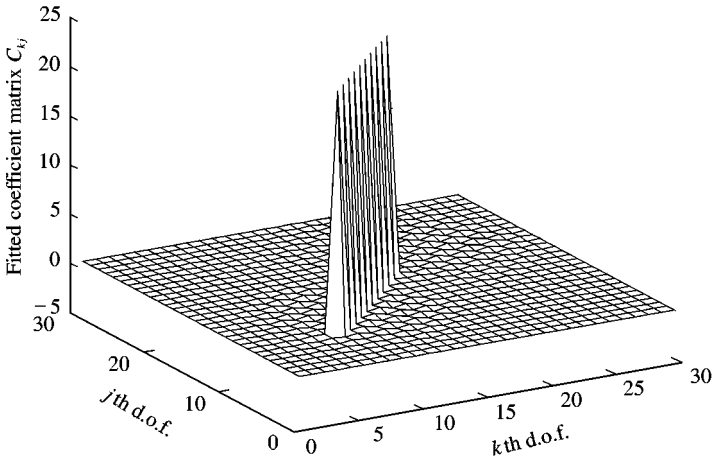
Figure 11. Fitted coefficient matrix of the exponential model for the local case, $\gamma = 0.5$, damping model 1.

[1], for damping model 1 (equation (22)) with locally reacting damping and the full set of 30 modes. Note that although fitting started with a locally reacting damping model, which means the true coefficient matrix is non-zero only along the diagonal, non-zero values in the off-diagonal terms show that the fitted viscous damping is, in a sense, not locally reacting. Figure 11 shows the corresponding result of fitting the exponential model for this problem. This result clearly demonstrates the improvement of fitting over the result in Figure 10. Since the damping model is "identified" correctly in this case, the correct value of the relaxation parameter is obtained, and the coefficient matrix corresponds to the exact coefficient matrix for the problem. Thus, even if the characteristic time constant of the damping mechanism present in a system is large, a correctly identified damping model can represent the true damping behaviour.

Figure 12(a) shows the fitted coefficient matrix of the exponential damping model similar to Figure 11 but with damping model 2 (equation (23)). The fitted matrix has some negative off-diagonal values which wrongly gives the impression that the damping type is non-local. For this result equation (21a) with $k = 1$ has been used to estimate the relaxation parameter. Figure 12(b) compares the original damping time function (Gaussian) with the fitted exponential function. It may be observed that although the fitted coefficient matrix does not match the original one very accurately the time functions agree with reasonable accuracy. Since $\hat{\gamma} = 0.4951$ the characteristic time constant of the fitted exponential model is surprisingly close to the exact γ of the simulated model. This remains true with even larger values of the characteristic time constant for systems with damping model 2.

The identification results show somewhat different behaviour for systems with damping model 3. Figure 13 shows the fitted coefficient matrix of the exponential function with $\gamma = 0.5$ for damping model 3 with two exponential functions as considered in section 3.3.2. Compared to the case of damping model 2 (Figure 12(a)), the fitted coefficient matrix is much closer to the original coefficient matrix used for simulation. However, note that for the fitted exponential function $\hat{\gamma} = 0.4834$, less close to the correct value than that obtained with damping model 2.

In the companion paper [1], it was shown that the features of the fitted viscous model were quite similar in the case of non-viscous damping models 1 and 2. Now, however, the features of fitting the exponential model with damping model 2 (Figure 12(a)) are clearly different from those with model 1 (Figure 11) and model 3 (Figure 13). This is due to the fact
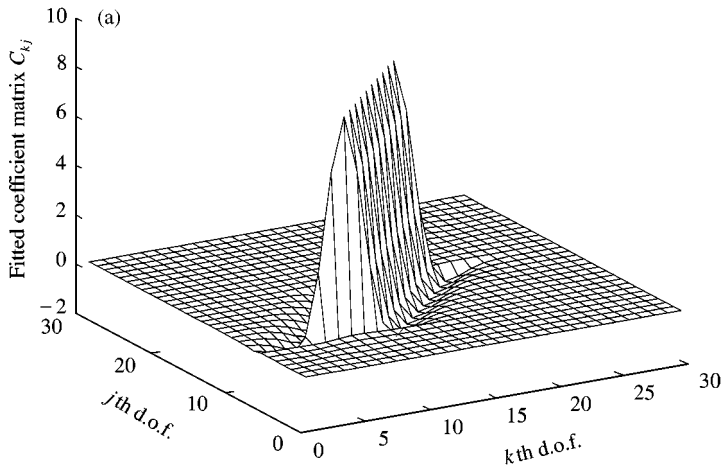
Figure 12. (a) Fitted coefficient matrix of the exponential model for the local case, $\gamma = 0.5$, damping model 2.
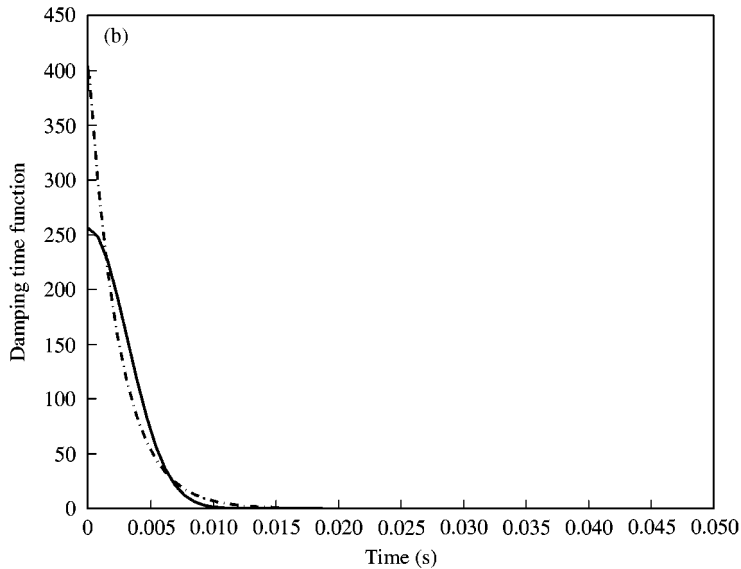
Figure 12. (b) Original and fitted damping time function for the local case with damping model 2: (———), original damping function, $\gamma = 0.5$; ($\cdot - - \cdot -$), fitted function, $\hat{\gamma} = 0.49507$.

that a viscous damping model was incorrect for both models 1 and 2, whereas when fitting the exponential model, it is correct for damping model 1 and close for damping model 3. For damping model 2, since the original damping function is Gaussian while the fitted function is exponential, the coefficient matrix does not correspond to the exact coefficient matrix of the problem. For damping model 3, the fitted exponential function seems to give a much better approximation to the original multiple exponential function, and the coefficient matrix is remarkably close to the "correct" values.

Finally, attention turns to the non-local case shown in Figure 1(b). As has just been shown with locally reacting damping, the proposed method can identify the exact coefficient
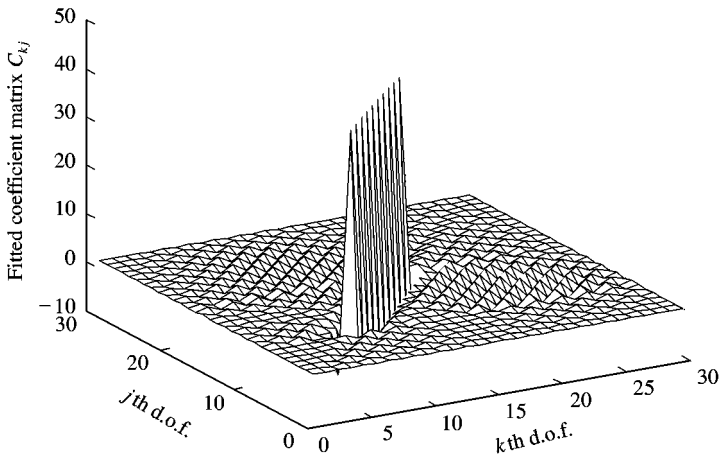
Figure 13. Fitted coefficient matrix of the exponential model for the local case, $\gamma = 0.5$, damping model 3.

matrix and damping function for the system with damping model 1 because the fitted model is the same as the original model. Figure 14 shows the fitted coefficient matrix for damping model 2, using the full set of 30 modes. For these results equation (21a) with $k = 1$ has been used to calculate $\hat{\gamma} = 0.5033$. Thus although the fitted coefficient matrix does not match very well with the original one, it is found once again that the value of the characteristic time constant is quite accurately predicted. For damping model 3 it was observed (results not shown) that, as in the locally reacting case, the identified coefficient matrix is very close to the original one.

It might be thought that a useful check on the accuracy of the fitting method could be made by comparing the "measured" and reconstructed transfer functions. However, little information is gained from such a comparison. The reason is that for both viscous and non-viscous fitting procedures, the poles and corresponding residues of all transfer functions are fitted correctly. It follows from Liouville's theorem that the transfer functions are always well reproduced. This demonstrates that there is a fundamental ambiguity in damping identification: two different damping models (e.g., the viscous model and the exponential model) with different spatial distributions and different sets of parameters can reproduce accurately the full set of transfer functions of a system with an entirely different damping model (e.g., the Gaussian model) with different spatial distributions and parameters. This in turn implies that *just by measuring the transfer functions it is not possible to identify uniquely the governing damping mechanism.* However, it should be noted that in cases like Figures 12(a), 14, etc., the fitted coefficient matrix is not symmetric. This is a non-physical result, which can be regarded as evidence that the true damping behaviour is not in fact described by an exponential function. In the companion paper [1] similar features were also observed while fitting a viscous damping matrix.

This appears to mean that it does not matter whether the right damping model is used, since a wrong model fits all the transfer functions just as well. This is, however, misleading. A common reason for constructing a theoretical model of vibration is in order to guide changes to the structure to reduce a vibration problem. If the wrong damping model is used, it is likely that prediction of the effect of structural changes will not be accurate. Conversely, if it is wished to develop a procedure to estimate more reliably the correct damping model, it would be necessary to introduce deliberate, controlled changes to the system in order to obtain the necessary additional experimental information.
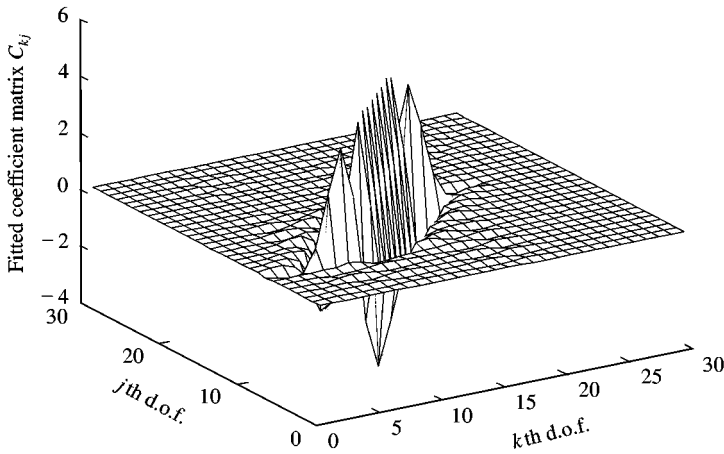
Figure 14. Fitted coefficient matrix of the exponential model for the non-local case, $\gamma = 0.5$, damping model 2.

5. CONCLUSIONS AND FURTHER RESEARCH

In this paper, a method has been proposed to identify a non-proportional non-viscous damping model in vibrating systems. It is assumed that damping is light so that the first order perturbation method is applicable. The method is simple, direct, and compatible with conventional modal testing procedures. The complex modes and natural frequencies are used together with the system mass matrix. The method does not require the full set of modal data. The damping behaviour is assumed to be described by an exponential relaxation function, and the relaxation time constant is found as part of the fitting procedure. Identification of the familiar viscous damping model is a special case of the general method proposed here. The validity of the proposed method has been explored by applying it to simulated data from a simple test problem, in which a linear array of spring-mass oscillators is damped by non-viscous elements over part of its length.

Numerical experiments have been carried out with a wide range of parameter values and different damping models. The main features of the results have been illustrated by two particular damping models and representative parameter values. It has been shown that the method generally predicts the spatial location of the damping with good accuracy, and also gives a good indication of whether the damping is locally reacting or not. In general, the relaxation time constant was fitted well, even when the coefficient matrix was less accurate. The transfer functions obtained from the fitted exponential damping model agree well with the exact transfer functions of the simulated system. Reciprocity of the transfer functions is preserved within an acceptable accuracy, although in some cases the fitted coefficient matrix is not symmetric, indicating that the true damping model differs from the assumed exponential model.

When the time constant is short compared with the periods of all modes retained in the analysis, the damping is close to viscous and the fitting procedure gives a physically sensible symmetric coefficient matrix and an accurate value of the relaxation parameter. When the time constant is larger, however, the memory of the damping function influences the detailed behaviour. If the identified model matches the true model then the fitting procedure

gives a correct physical description of the damping. When the models are different, the poles and residues of the transfer functions are still fitted accurately with a model of the form considered, but the underlying different functional behaviour manifests itself in a non-symmetrical coefficient matrix and significant variation of fitted relaxation parameter with mode number. A correct physical description of the damping mechanism can be obtained only if a correct model is selected and fitted.

From equation (5) it can be deduced that, within the approximation of small damping, each frequency function $G'_{kj}(\omega)$ can be observed at only two frequencies, ω_j and ω_k. This fact imposes a fundamental restriction on identification of an exact damping function using this approach. When the fitted coefficient matrix turns out to be non-symmetric, this indicates that it was not possible to fit the assumed function through both "measured" frequency points, and two different coefficients were needed. To correct this problem it would be necessary to fit a different damping model, able to pass through both measured points while retaining symmetric coefficients. The function cannot be uniquely determined by this requirement, of course. There can be two possible ways to tackle this problem. Different physically plausible damping models can be "inverted" and attempts can be made to fit their parameters using the approach outlined in this paper and see which model fits the measured data most convincingly. Alternatively, the viscous or exponential model might be used and constraints put on the coefficients such that they yield symmetric coefficient damping matrix. Research is currently in progress to explore these questions.

There are a number of interesting issues, which will be addressed in future works. Most immediate of these are experimental testing of the prediction and analysis of the effect of measurement errors on the procedure. After that, there is scope to extend the study to two-dimensional systems, systems with joints, etc.

REFERENCES

1. S. ADHIKARI and J. WOODHOUSE 2000 *Journal of Sound and Vibration* **243**, 43–61. Identification of damping: Part 1, viscous damping.
2. B. J. LAZAN 1968 *Damping of Materials and Members in Structural Mechanics*. Oxford: Pergamon Press.
3. C. W. BERT 1973 *Journal of Sound and Vibration* **29**, 129–153. Material damping: an introductory review of mathematical models, measure and experimental techniques.
4. E. E. UNGAR 1973 *Journal of Sound and Vibration* **26**, 141–154. The status of engineering knowledge concerning the damping of built-up structures.
5. A. D. NASHIF, D. I. G. JONES and J. P. HENDERSON 1985 *Vibration Damping*. New York: John Wiley.
6. V. BABURAJ and Y. MATSUKAI 1994 *Journal of Sound and Vibration* **172**, 415–419. A study on the material damping of thin angle-ply laminated plates.
7. S. ADHIKARI 2000 *Ph.D. Thesis, Cambridge University Engineering Department, Cambridge, UK*. Damping Models for Structural Vibrations.
8. S. W. E. EARLS 1966 *Journal of Mechanical Engineering Science* **8**, 207–214. Theoretical estimation of frictional energy dissipation in a simple lap joint.
9. C. F. BEARDS and J. L. WILLIAMS 1977 *Journal of Sound and Vibration* **53**, 333–340. The damping of structural vibration by rotational slip in structural joint.
10. J. P. BANDSTRA 1983 *Journal of Vibration Acoustics Stress and Reliability in Design* **105**, 382–392. Comparison of equivalent viscous damping in discrete and continuous vibrating systems.

11. H. T. Banks and D. J. Inman 1991 *ASME Journal of Applied Mechanics* **58**, 716–723. On damping mechanisms in beams.
12. J. Fang and G. J. Lyons 1994 *Journal of Sound and Vibration* **172**, 371–389. Material damping of free hanging pipes: theoretical and experimental studies.
13. J. Woodhouse 1998 *Journal of Sound and Vibration* **215**, 547–569. Linear damping models for structural vibration.
14. M. A. Biot 1958 *Proceedings of the* 3rd *U.S. National Congress on Applied Mechanics* 1–18. New York: ASME, Linear thermodynamics and the mechanics of solids.
15. L. Cremer and M. Heckl 1973 *Structure-Borne Sound*. Berlin, Germany: Springer-Verlag, second edition. Translated by E. E. Ungar.
16. A. Muravyov 1997 *Journal of Sound and Vibration* **199**, 337–348. Analytical solutions in the time domain for vibration problems of discrete viscoelastic systems.
17. Lord Rayleigh 1877 *Theory of Sound* (2 *vols.*) New York: Dover Publications, 1945 re-issue, second edition.

APPENDIX A: SELECTING THE VALUE OF $\hat{\mu}$

From equations (21a)–(21c) it is clear that different choices of j yield different values of $\hat{\mu}$, which contradicts the initial assumption that the system has only one relaxation time. Here it will be shown that for systems with normalized damping functions similar to equations (22) and (23) the best estimate of $\hat{\mu}$ is given by equation (21a) with $k = 1$.

Since the damping functions are normalized to have unit area when integrated to infinity they can be written in the form

$$g(t) = \beta f(t) \quad \text{where} \quad \beta = \frac{1}{\int_0^\infty f(t)\,dt}. \tag{A.1}$$

The characteristic time constant is obtained from equation (26) as

$$\theta = \frac{\int_0^\infty t f(t)\,dt}{\int_0^\infty f(t)\,dt}. \tag{A.2}$$

It is useful to express this result in the frequency domain. From the definition of the Fourier transform

$$F(\omega) = \int_0^\infty f(t)\,e^{-i\omega t}\,dt, \tag{A.3}$$

differentiating with respect to ω gives

$$F'(\omega) = \frac{dF(\omega)}{d\omega} = \int_0^\infty -i\,t f(t)\,e^{-i\omega t}\,dt. \tag{A.4}$$

From equations (A.3) and (A.4) it is clear that

$$F(0) = \int_0^\infty f(t)\,dt, \quad \text{and} \quad iF'(0) = \int_0^\infty t f(t)\,dt \tag{A.5}$$

so that from equation (A.2) the characteristic time constant may be represented as

$$\theta = \frac{iF'(0)}{F(0)}. \tag{A.6}$$

Substituting $g(t)$ from (A.1) and taking the Fourier transform of equation (6) gives

$$\mathbf{G}(\omega) = \mathbf{C}\,\beta F(\omega) = \mathbf{C}\,\beta\,[F_R(\omega) + i\,F_I(\omega)], \tag{A.7}$$

where

$$F(\omega) = F_R(\omega) + i\,F_I(\omega), \tag{A.8}$$

where F_R and F_I are, respectively, the real and imaginary parts of F. Using this $\mathbf{G}(\omega)$ in the approximate expression for the complex modes in equation (5) and separating real and imaginary parts gives

$$\mathbf{u}_j = \Re(\mathbf{z}_j) \approx \mathbf{x}_j - \omega_j \beta F_I(\omega_j) \sum_{\substack{k=1 \\ k \neq j}}^{N} \frac{C'_{kj}}{(\omega_j^2 - \omega_k^2)}\,\mathbf{x}_k \tag{A.9}$$

and

$$\mathbf{v}_j = \Im(\mathbf{z}_j) \approx \omega_j \beta F_R(\omega_j) \sum_{\substack{k=1 \\ k \neq j}}^{m} \frac{C'_{kj}}{(\omega_j^2 - \omega_k^2)}\,\mathbf{x}_k. \tag{A.10}$$

From the above two equations it is easy to see that

$$\mathbf{u}_j = \mathbf{x}_j - \frac{F_I(\omega_j)}{F_R(\omega_j)}\,\mathbf{v}_j. \tag{A.11}$$

It has been mentioned that $\hat{\mathbf{v}}_j$ is $\mathbf{M}$-orthogonal to its corresponding undamped mode, i.e., $\hat{\mathbf{v}}_j^{\mathrm{T}}\mathbf{M}\hat{\mathbf{x}}_j = 0$. Using this relationship in equation (A.11) yields

$$\mathbf{v}_j^{\mathrm{T}}\mathbf{M}\mathbf{u}_j = -\frac{F_I(\omega_j)}{F_R(\omega_j)}\,\mathbf{v}_j^{\mathrm{T}}\mathbf{M}\mathbf{v}_j \quad \text{or} \quad \frac{\mathbf{v}_j^{\mathrm{T}}\mathbf{M}\mathbf{u}_j}{\mathbf{v}_j^{\mathrm{T}}\mathbf{M}\mathbf{v}_j} = -\frac{F_I(\omega_j)}{F_R(\omega_j)}. \tag{A.12}$$

From this equation, the expression for $\hat{\mu}$ may be rewritten as

$$\hat{\mu} = -\frac{\hat{\omega}_j F_R(\hat{\omega}_j)}{F_I(\hat{\omega}_j)}. \tag{A.13}$$

For the exponential function it has been shown that the characteristic time constant $\theta = 1/\mu$. Thus, using equation (A.6)

$$\mu = \frac{1}{\theta} = \frac{-i\,F(0)}{F'(0)}. \tag{A.14}$$

This is an exact relationship. It is now shown why equation (A.13) is a good approximation to equation (A.14) when ω_j is small. Since $f(t)$ is a real function $F(\omega)$ can be expanded as a real polynomial in $(i\,\omega)$. Thus,

$$F(\omega) = F^{(0)} + (i\omega)\,F^{(1)} + \frac{(i\omega)^2}{2!}\,F^{(2)} + \cdots, \tag{A.15}$$

where all $F^{(k)}$ are real. From this expansion

$$F(0) = F^{(0)}, \quad F'(0) = i\,F^{(1)}. \tag{A.16}$$

Now, consider the case when ω is *small*. For this case, the higher order terms in series (A.15) can be neglected to obtain

$$F(\omega) \approx F^{(0)} + \mathrm{i}\omega F^{(1)}. \tag{A.17}$$

Comparing above with equation (A.8) and in view of (A.16) gives

$$F_R(\omega) \approx F(0) = F^{(0)} \quad \text{and} \quad F_I(\omega) \approx \omega F^{(1)} = -\mathrm{i}\omega F'(0). \tag{A.18}$$

Substituting in equation (A.14) gives

$$\mu \approx -\frac{\omega F_R(\omega)}{F_I(\omega)} \quad \text{when} \quad \omega \to 0. \tag{A.19}$$

This result is immediately comparable with the expression for $\hat{\mu}$ in (A.13). Observe that $\hat{\omega}_j$ is closest to zero when $j = 1$. For this reason, the best estimate of $\hat{\mu}$ can be obtained by choosing $j = 1$ in equation (A.13). From equation (A.12) this in turn implies that

$$\hat{\mu} \approx -\frac{\hat{\omega}_1 F_R(\hat{\omega}_1)}{F_I(\hat{\omega}_1)} = \frac{\hat{\omega}_1 \hat{\mathbf{v}}_1^{\mathrm{T}} \mathbf{M} \hat{\mathbf{v}}_1}{\hat{\mathbf{v}}_1^{\mathrm{T}} \mathbf{M} \hat{\mathbf{u}}_1}. \tag{A.20}$$

APPENDIX B: NOMENCLATURE

$\mathbf{C}$	viscous damping matrix
$D(t)$	energy dissipation function
$D(\omega)$	Fourier transform of $\mathscr{D}(t)$
$f(t)$	non-viscous damping functions (not normalized)
$F(\omega)$	Fourier transform of $f(t)$
$F_R(\omega)$	real part of $F(\omega)$
$F_I(\omega)$	imaginary part of $F(\omega)$
$\mathscr{G}(t)$	damping function matrix in the time domain
$g(t)$	normalized non-viscous damping functions
$\mathbf{G}(\omega)$	Fourier transform of damping function matrix $\mathscr{G}(t)$
$G(\omega)$	Fourier transform of damping function $g(t)$
$G_R(\omega)$	real part of $G(\omega)$
$G_I(\omega)$	imaginary part of $G(\omega)$
$\mathbf{G}'(\omega)$	frequency domain damping function matrix in the modal co-ordinates
$H_{ij}(\omega)$	set of measured transfer functions
$\mathbf{K}$	stiffness matrix
m_μ	number of modes used for estimation of $\hat{\mu}$
$\mathbf{M}$	mass matrix
$\mathscr{M}_k$	kth moment of $g(t)$
N	degrees of freedom of the system
m	number of measured modes
Q_j	Q-factor for the jth mode
t	time
T_{min}	minimum time period for the system
$\mathbf{x}_j$	jth undamped mode
$\mathbf{X}$	matrix containing $\mathbf{x}_j$
$\mathbf{y}(t)$	vector of the generalized co-ordinates
$\mathbf{z}_j$	jth complex mode
$\hat{\mathbf{z}}_j$	jth measured complex mode
$\hat{\mathbf{U}}$	matrix containing $\hat{\mathbf{z}}_j$
$\hat{\mathbf{u}}_j$	real part of $\hat{\mathbf{z}}_j$
$\hat{\mathbf{U}}$	matrix containing $\hat{\mathbf{u}}_j$
$\hat{\mathbf{v}}_j$	imaginary part of $\hat{\mathbf{z}}_j$

$\hat{\mathbf{V}}$	matrix containing $\hat{\mathbf{v}}_j$
ω_j	jth undamped natural frequency
λ_j	jth complex natural frequency of the system
ε_j	error vector associated with the jth complex mode
$\alpha_l^{(j)}$	constants associated with expansion of the jth elastic modes
ζ_j	jth modal damping factor
μ	relaxation parameter of the fitted damping model
$\hat{\mu}_j$	estimated relaxation parameter for the jth mode
μ_1	constant associated with exponential damping function
μ_2	constant associated with Gaussian damping function
μ_3, μ_4	constants associated with double exponential damping function
β_1, β_2	weights associated with double exponential damping function
β	normalization constant associated with non-viscous damping function, $f(t) = \beta g(t)$
$\hat{\theta}_j$	estimated characteristic time constant for the jth mode
$\hat{\theta}(\omega)$	frequency-dependent estimated characteristic time constant
θ	characteristic time constant
γ	non-dimensional characteristic time constant
$\delta(t)$	Dirac-delta function
$\mathbb{C}$	space of complex numbers
$\mathbb{R}$	space of real numbers
$\Re(\bullet)$	real part of $(\bullet)$
$\Im(\bullet)$	imaginary part of $(\bullet)$
$\hat{(\bullet)}$	estimated value of $(\bullet)$
$(\bullet)^{\mathrm{T}}$	matrix transpose of $(\bullet)$
$(\bullet)^{-1}$	matrix inverse of $(\bullet)$
$\dot{(\bullet)}$	derivative of $(\bullet)$ with respect to t
$(\bullet)^*$	complex conjugate of $(\bullet)$